ACS Photonics

Article

pubs.acs.org/journal/apchd5

Plasmon-Assisted Designable Multi-Resonance Photodetection by Graphene via Nanopatterning of Block Copolymer

Un Jeong Kim,[†,‡] Seungmin Yoo,[‡,§] Yeonsang Park,[†] Myoungsoo Shin,[§] Jineun Kim,[†] Heejeong Jeong,[†] Chan-Wook Baik,[†] Young-Geun Roh,[†] Jaesoong Lee,[†] Kyuhyun Im,[†] Hyungbin Son,[∥] Sungwoo Hwang,[†] Chang-Won Lee,*[,†] and Soojin Park*[,§]

[†]Nano Electronics Lab. Samsung Advanced Institute of Technology, Suwon, Gyeonggi-Do 446-712, South Korea

[§]Department of Energy Engineering, School of Energy and Chemical Engineering, Ulsan National Institute of Science and Technology (UNIST), Ulsan 689-798, South Korea

[∥]School of Integrative Engineering, Chung-Ang University, Seoul 156-756, South Korea

Supporting Information

ABSTRACT: The photoresponse in graphene has drawn significant attention for potential applications owing to its gapless linear electronic band structure. To enhance both the spectral selectivity and responsivity in graphene, we demonstrate a novel but versatile and simple method of introducing surface plasmons. We utilize block copolymers to fabricate different nanostructured metal nanoparticle arrays on a single graphene surface. The plasmonic resonances could be tuned using Ag, Au, and Cu metal nanoparticles. By extending the synthetic route for the metallic particles, dual surface plasmonic bands from a single material were also successfully realized. Furthermore, enhanced photoresponsivity through the entire visible spectra could be achieved by mixing metallic nanoparticles and by controlling their shapes. Owing to its all-band transition characteristics, the ultrabroad band photocurrent generation in graphene can be tailored for an arbitrary photoresponse, which could be utilized in flexible CMOS image sensors (CIS) or other optoelectronic devices in the future.

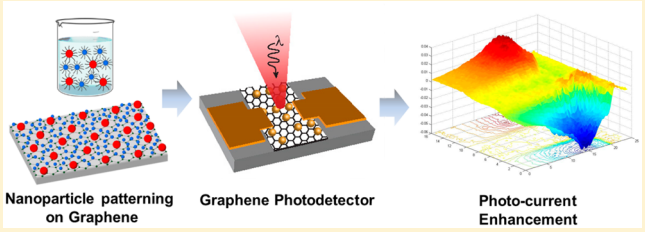

KEYWORDS: *photodetector, graphene, block copolymer, metal nanoparticle, surface plasmon*

Graphene, a two-dimensional network of carbon atoms in a honeycomb lattice, has been intensively studied for the past decade owing to its unique optical and electronic properties in both fundamental science and applications.[1−6] Numerous studies have proven that the linear, gapless band structure of graphene surpasses the performance of currently available semiconductor-based electronic and optical devices on the market; in other words, unlike other superconductors, the ultrahigh mobility[1,7] and ultrabroad-band photoresponse originated by the all-band transition in graphene can be substantially modified through electrical gating.[8,9]

Photocurrent generation in graphene has been observed at the graphene/metallic electrode junction,[10−12] at the *p*-/*n*-junction formed on graphene by top gating,[12−14] and at the interface of graphene and various materials in the heterostructure.[15−24] Graphene-based interband photodetectors have been demonstrated from the ultraviolet, visible to mid-infrared (mid-IR) range, covering all optical communication bands.[16] Photocurrent at the metal−graphene junction and graphene *p*−*n* junctions has been described as either photovoltaic[10,12] or thermoelectric.[25] However, it is challenging to identify photovoltaic and thermoelectric currents in metal−graphene or graphene p−n junctions due to its identical polarity. Recently, in biased graphene, the thermoelectric effects are insignificant, but the photovoltaic and photoinduced bolometric effects dominate the photoresponse.[12]

The property of the linearly dispersive and zero band gap, however, leads to a low density of states and no spectral selectivity. Therefore, there have been efforts to improve the low responsivity of graphene-based photodetectors by enhancing the light absorption with the aid of localized surface plasmon enhancement[26−28] or by near-field coupling with guided waveguides.[20−22] Recently, the responsivity was significantly increased by 3 orders of magnitude over that of typical graphene-based photodetectors by introducing electron-trapping centers and by creating a band gap in graphene by holely quantum dot forming.[29] The responsivity was also significantly increased in the phototransistor structure consisting of a pair of stacked graphene monolayers separated by a thin tunnel barrier.[23] Recently, photoresponse in reduced graphene oxide (rGO) was studied in the infrared range.[24] By controlling defects and atomic structure by thermal reduction, responsivity was obtained as high as 0.7 A/W, which is over 1 order of magnitude higher than that from pristine graphene.[24] The lack of spectral selectivity originating from the near-

Received: October 31, 2014
Published: March 3, 2015

DOI: 10.1021/ph500412p
ACS Photonics 2015, 2, 506−514

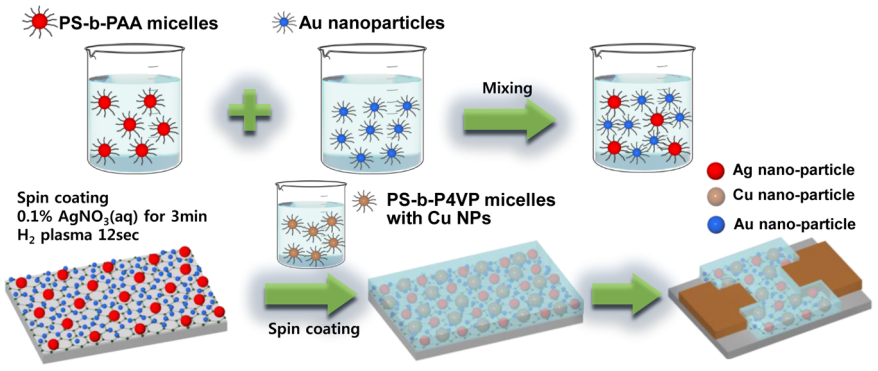

Figure 1. Schematic illustration showing the fabrication process of the plasmonic-enhanced multiband graphene photodetector. (a) The Ag-precursor-containing PS-*b*-PAA spherical micelles and the oleylamine-decorated Au nanoparticles are mixed together. (b) A mixture of PS-*b*-PAA(Ag) and Au is spin-coated on the graphene surface. Subsequently, the Cu nanoparticle-loaded PS-*b*-P4VP micellar thin films are coated onto Ag/Au arrays to form the triple-band graphene photodetector.

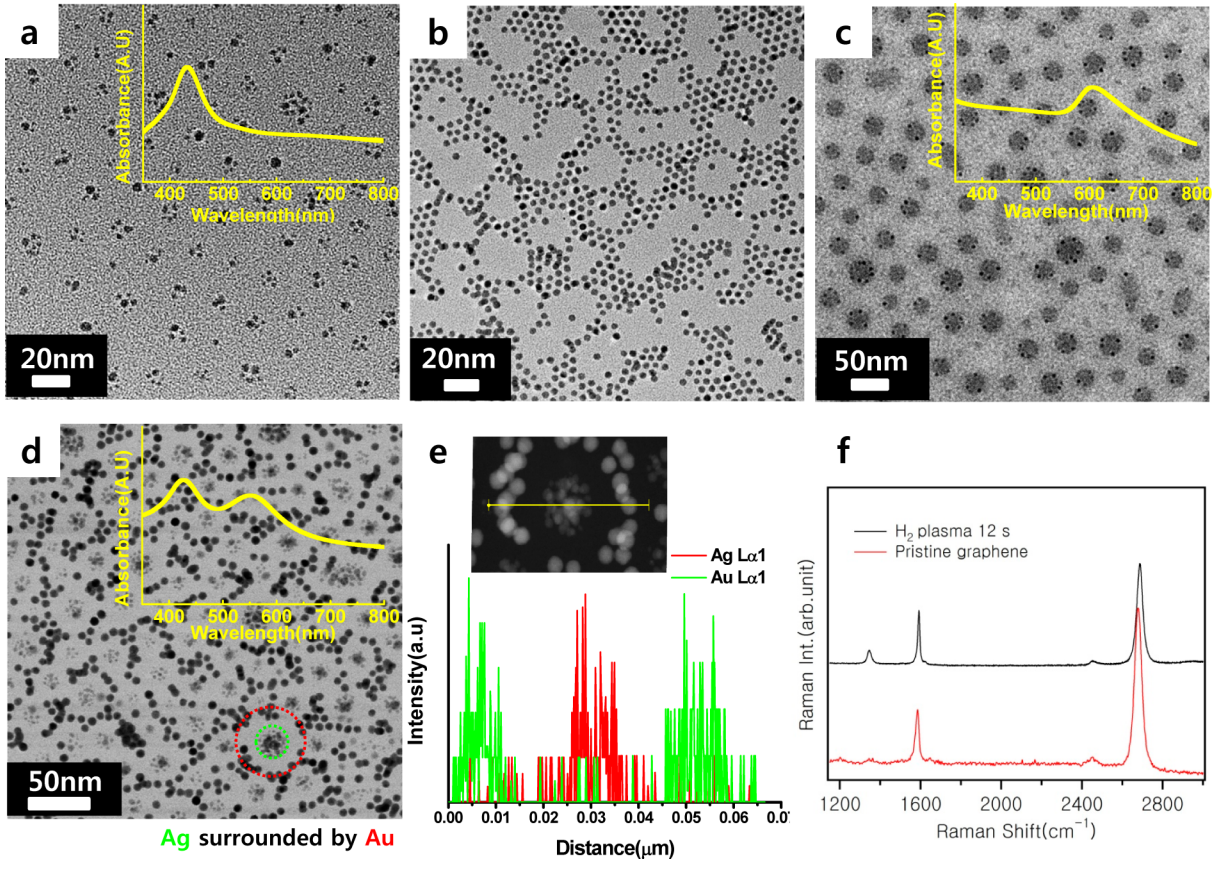

Figure 2. Characteristics of the block copolymer-templated metal nanoparticle arrays. (a) A TEM image of the Ag nanoparticle arrays fabricated by PS-*b*-PAA micelles. Inset shows a typical surface plasmon band of Ag nanoparticles. (b) A TEM image of the Au nanoparticle arrays spatially located around the PS-*b*-PAA micelles without Ag. (c) A TEM image of the Cu nanoparticle-loaded PS-*b*-P4VP micelles. Inset shows a surface plasmon peak of the Cu nanoparticles at ~610 nm. (d) A TEM image of the Au and Ag nanoparticle arrays. Spatial locations of Au (dotted green) and Ag (dotted red) particles are indicated with visual aids. Inset shows dual surface plasmon bands exhibiting from the Au and Ag particles. (e) A HADDF-STEM image of the Au/Ag patterned arrays and a line-scan profile showing the spatial location of each nanoparticle. (f) The Raman spectra of pristine graphene and Ag-patterned graphene.

resonant interband transition has been overcome by introducing additional metallic nanostructures on graphene[26−28] or by introducing colloidal PbS quantum dot/graphene hybrid structures showing a high responsivity up to ~10^7 A/W at the infrared wavelength.[17,18] By taking advantage of the plasmonic resonance by patterning metal nanostructures on graphene, both high responsivity and spectral selectivity can be achieved.

In the literature, metallic nanostructures have typically been fabricated either by photolithography or by electron-beam lithography. However, these methods can be limited when nonconducting substrates are required or when multiple plasmonic band enhancements are necessary for graphene-based photodetectors. Block copolymers (BCPs), which self-assemble into arrays with nanosized domains, are good candidates because they can be used as templates and scaffolds

DOI: 10.1021/ph500412p
ACS Photonics 2015, 2, 506−514

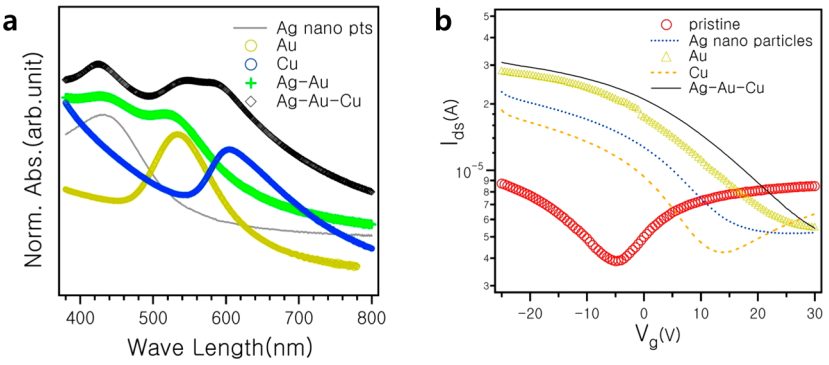

Figure 3. Optical absorbance and electrical properties of metal-decorated graphene devices. (a) The UV−vis absorption spectra of isolated metal nanoparticle arrays, Ag/Au dual patterns, and Ag/Au/Cu triple-patterned arrays. (b) The I_{ds}−V_{gs} curves of pristine graphene, Ag, Au, and Cu metal nanoparticle-patterned graphene, and the triple component (Ag−Au−Cu)-decorated graphene transistor at V_{ds} = 10 mV.

for fabricating arrays of nanoscopic metal elements. Moreover, nanostructured BCP thin films can be formed over arbitrary substrates such as silicon, quartz, plastic, and graphene by controlling the substrate surface energy and by selecting a suitable solvent.[31−33]

Herein, conventional block copolymers are utilized to fabricate nanostructured metal nanoparticle arrays on graphene. This protocol is very simple and versatile for tuning the plasmonic resonance and controlling the number of resonances. Arrays of silver, gold, and copper nanoparticles, which have different surface plasmomic bands, are fabricated on graphene substrates to make plasmonic-enhanced multiband photodetectors. Graphene-based photodetectors plasmonically enhanced in the red/green/blue region may be utilized for color filters. A flexible CMOS image sensor (CIS) could be one of the promising applications of graphene photodetectors assisted with plasmonic enhancement in the near future, which simultaneously fulfills the functions of a color filter. By tuning the number and the frequency of plasmonic resonances by utilizing block copolymers, multiband graphene-based photodetectors could be applied to various applications in the future.

RESULTS AND DISCUSSION

Figure 1 describes the fabrication process for our plasmonic-enhanced multiband graphene photodetector by fabricating metal nanoparticle arrays using directed self-assembly of BCP thin films. To demonstrate plasmonically enhanced multibands containing red (650 nm)/green (550 nm)/blue (450 nm) bands, the BCP-template-based copper/gold/silver (Cu/Au/Ag) nanoparticles are arranged on graphene. First, BCP spherical micelles are formed in toluene, which is a preferential solvent for one of the BCP components, and mixed with as-synthesized oleylamine-modified Au nanoparticles. Subsequently, the BCP micelles/Au are transferred onto a graphene transistor to form a hierarchical self-assembly of Au nanoparticles and BCP micelles. Second, functional group-containing BCP thin films are immersed in an aqueous $AgNO_3$ solution to form Ag nanoparticle arrays surrounded by Au nanoparticles. Third, the Cu nanoparticle-loaded BCP micellar thin films are coated on nanostructured Au/Ag patterns to fabricate three isolated Cu/Au/Ag arrays for triple surface plasmon bands. The final form of the sample is a graphene sheet with three metal nanoparticle arrays for plasmonic-enhanced multiband photodetectors.

Typically, 0.5 wt % polystyrene-*block*-poly(acrylic acid) (PS-*b*-PAA) copolymers (number-average molecular weight of 20.3 kg/mol) were dissolved in toluene, which is a selective solvent for the PS block, to make spherical micelles consisting of a PS corona and a PAA core. Subsequently, the PS-*b*-PAA micelles were transferred onto a Formvar-coated copper grid to create quasi-hexagonal arrays of PAA spheres within a PS matrix (see Supporting Information, Figure S1). When the PS-*b*-PAA thin films were immersed in an aqueous $AgNO_3$ solution, the carboxylic acid groups in the PAA domains can be used to selectively sequester Ag cations.[34] Subsequent hydrogen plasma treatment for a short time (12 s) led to the fabrication of Ag nanoparticle arrays without changing the separation distance of original PS-*b*-PAA micelles (Figure 2a).

In the next step, we synthesized oleylamine-modified Au nanoparticles according to a previous report.[35] The as-synthesized Au nanoparticles with an average diameter of 5 nm are mixed with the PS-*b*-PAA micellar solution and transferred onto a silicon nitride window to obtain the transmission electron microscopy (TEM) image. Figure 2b shows that the Au nanoparticles are spatially located around the micelles, which are not shown because of the low electron contrast in TEM. Note that the oleylamine ligand plays an important role in the dispersion of Au nanoparticles in toluene and in the Au nanoparticle repulsion from the PS corona, forming isolated Au nanoparticle arrays separated from BCP micelles.

To fabricate Cu nanoparticle arrays, we employed polystyrene-*block*-poly(4-vinylpyridine) (PS-*b*-P4VP, number-average molecular weight of 53.5 kg/mol) spherical micelles dissolved in toluene, which is a selective solvent for PS. Because a rich variety of metal salts can be selectively coordinated to the P4VP blocks,[36,37] copper chloride ($CuCl_2$) was dissolved in the PS-*b*-P4VP micelles (molar ratio of $CuCl_2$/vinylpyridine of 0.8). The resulting mixture was subsequently added to the reducing agent hydrazine in order to make Cu nanoparticles within micellar cores. Figure 2c shows that Cu nanoparticles with an average diameter of 5 nm are clearly seen within the P4VP domains. However, nanostructured Cu nanoparticle arrays were not easily obtained at room temperature because of the relatively low reduction potential of Cu compared to that of other novel metals.[38] Therefore, we added the reducing agent into the Cu-precursor loaded PS-*b*-P4VP micelles at a high temperature of 80 °C. Surface plasmon bands of three metal nanoparticles are seen in the inset of Figure 2a−c. The Ag, Au, and Cu nanoparticle arrays show typical plasmon bands at wavelengths (λ_{max}) of 420, 520, and 610 nm, respectively, which coincides with that given in previous reports.[39] High-resolution

DOI: 10.1021/ph500412p
ACS Photonics 2015, 2, 506−514

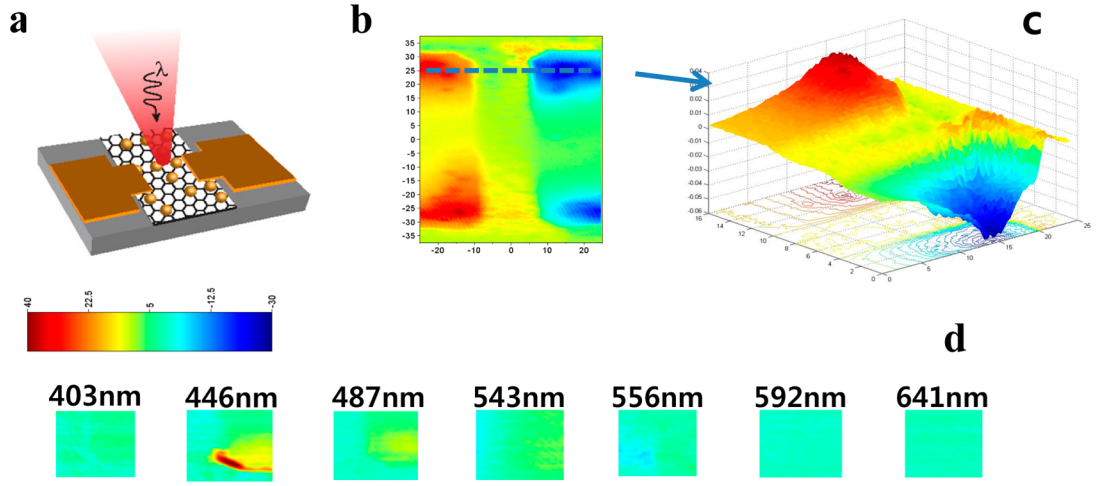

Figure 4. Photocurrent mapping. (a) Schematics of the photocurrent mapping of the nanoparticle decorated graphene device. (b) Photocurrent mapping image of the Ag nanoparticle decorated graphene transistor with 487 nm laser with 200 nm per step at zero gate and drain bias. (c) A 3D plot of the photocurrent image along the dashed line in (b). (d) Photocurrent mapping image of at the edge of electrode of the Ag nanoparticle decorated graphene transistors at various laser wavelength with 200 nm per step at zero gate and drain bias.

TEM (HR-TEM) images show highly crystalline Ag, Au, and Cu nanoparticles (Supporting Information, Figure S2).

In order to fabricate a system with dual surface plasmon bands, the PS-*b*-PAA/Au samples (shown in Figure 2b) were immersed in an aqueous $AgNO_3$ solution, which was followed by hydrogen plasma treatment. Figure 2d shows that the hierarchical self-assembled nanostructures, which are Au nanoparticle arrays surrounded by Ag nanoparticles, are successfully fabricated (Figure 2d) and exhibit dual surface plasmon bands that originate from the Ag and Au nanoparticles (Inset of Figure 2d). We confirmed that the Ag and Au nanoparticles were not in contact with each other, as evidenced by the high angle annular dark field-scanning transmission electron microscopy (HADDF-STEM) measurements. The line scan profile of energy dispersive X-ray spectroscopy (EDS) taken from the STEM image (selected area in Figure 1d) indicated that the Ag nanoparticles were surrounded by Au nanoparticles (Figure 2e).

To optimize the plasma treatment condition, which is a key step for metalizing precursors and removing the copolymer layers deposited on graphene, Raman spectroscopy is chosen to monitor the quality of the graphene. Bare graphene exhibits two distinctive modes at ~1582 cm^{-1} (below 1600 cm^{-1}) and ~1350 cm^{-1}, which are the G and D band, respectively. A third mode in the high-frequency region (~2700 cm^{-1}) is denoted as the 2D band. By using the intensity ratio of the D band over the G band, which is a commonly used "quality factor" to evaluate the condition of graphene, we found that hydrogen plasma treatment for about 12 s was enough to maintain the graphene crystallinity and to metalize the precursors (Figure 2f).

Figure 3a exhibits the normalized optical absorption spectra in the visible range to the highest intensity of graphene fabricated with arrays of single/double/triple metal nanoparticles. The spectra are cascaded for better visibility. The Ag (gray), Au (yellow), and Cu (blue) nanoparticles patterned on graphene exhibit localized surface plasmon resonances at approximately 420, 520, and 610 nm, respectively, which is consistent with that shown in previous reports.[39]

Simulations were performed using the finite-difference time-domain (FDTD) method (Lumercial FDTD solution).[40] The FDTD method is a rigorous numerical technique for solving the Maxwell equations in the time-domain. In this simulation, the optical absorption was calculated with the structure of graphene and metal particle arrays on the glass substrate. For the simulation, the diameter of metal particles and the center-to-center distance between the nanoparticles was taken to be 6 and 24 nm, respectively. These values were taken from the actual data based on atomic force microscopy (AFM) imaging. From the simulation, the Au, Ag, and Cu particles on graphene exhibit peaks at ~490, 510, and 620 nm, respectively, which are in good agreement with most of experimental results. In the Ag case shown in Figure 3, we observed a significant difference between the calculation and experimental results of about 50 nm. We speculate that this difference originates from the oxidation of the Ag nanoparticle surface formed by the block copolymer method (Supporting Information, Figure S3).

So far, single surface plasmon resonance is shown to be tuned by selecting materials. By multiple selection of materials and corresponding synthetic routes can effectively adjust the number and position of spectral resonance. Double surface plasmon bands were prepared by Ag nanoparticles surrounded by Au nanoparticles on graphene, as shown in Figure 1. By spreading the Cu nanoparticles embedded in PS-*b*-P4VP micelles on top of the Ag/Au nanoparticle arrays on graphene, a triple-band structure is now formed, as shown in Figure 3a (black line). The PS-*b*-P4VP provides a protective layer against the oxidation of Cu nanoparticles. To adjust the relative intensity of optical absorbance from each metal, the ratio among metal concentration was varied. According to the studies, Ag nanoparticles, and Cu nanoparticles produced the strongest and weakest localized surface plasmon peak, respectively, among Ag, Au, and Cu nanoparticles. We have found that the relative concentration of Ag/Au/Cu = 1:4:5 produces similar optical absorbance intensity at the resonance wavelengths. As shown in Figure 3a, for double band from Au–Ag metal nanoparticles (green cross) and triple band from Au–Ag–Cu metal nanoparticles (black diamond), weight ratio of 1:3 = Ag/Au and 1:4:5 = Ag/Au/Cu are found to produce similar optical absorbance intensity at the resonance wavelengths, respectively.

The graphene patterned with metal nanoparticle arrays is fabricated into a back-gate field effect transistor (FET), as

DOI: 10.1021/ph500412p
ACS Photonics 2015, 2, 506–514

shown in Figure 1. The dependence of the drain current (I_{ds}) on the gate voltage (V_g) was measured at V_{ds} = 10 mV under air. Graphene transistors exhibit ambipolar characteristics induced by the electron and hole current depending on the gate bias.[4,5] The field effect mobility (μ_{TFT}) in the linear regime was obtained using the standard formula, $\mu_{TFT} = (dI_d/dV_g)/(\varepsilon\varepsilon_0 V_{ds} W/Lt_{ox})$, where I_d is the drain−source current, V_g is the gate voltage, V_{ds} is the drain−source voltage, and t_{ox} is the thickness of SiO_2 (100 nm). The channel length (L) and width (W) were 5 and 45 μm, respectively. The electron (hole) mobility was ∼5800 (1100) $cm^2/(V\ s)$. These values were comparable to those of exfoliated graphene.[4,5] The transistors of graphene patterned with single component (Ag, Au, Cu) or triple component (Ag−Au−Cu) metal nanoparticles exhibited p-type doping characteristics. We observed a shift in the Dirac point toward the positive gate voltage, as shown in Figure 3b. Graphene can be n-type or p-type doped by the adsorption of metal particles. In the theoretical calculation, Ag, Au, Cu, and Pt (111) form weak bonds (0.04 eV per carbon atom) to graphene with a relatively large equilibrium separation (d_{eq} ∼ 3.3 Å), compared to Co, Ni, and Pd(111).[41] At the equilibrium separation between graphene and the metal surface, the graphene is n-type doped with Ag and Cu, and *p*-type doped with Au, which does not agree with our results. However, graphene can exhibit p-type doping even with Ag and Cu,[41] because of the distance between the graphene and metal. The large separation between graphene and metal nanoparticles over equilibrium separation is attributed to a thin, residual hydrophobic polymer (>1 nm) that is formed in between the graphene and metal nanoparticles, which leads to a positive voltage shift of the Dirac point by the Ag and Cu nanoparticles. We confirmed the existence of residual polymer layers beneath the Ag particles through X-ray photoelectron spectroscopy analysis (Supporting Information, Figure S4).

To study the photoresponse of the various metal nanoparticle-patterned graphene transistors, a focused laser beam was irradiated and scanned in the area of the device channel, including the area of the source and drain electrode at zero gate (V_g = 0 V) and drain bias (V_{ds} = 0 V). Figure 4 provides an overview of the characterization of photocurrent enhancement of the Ag nanoparticle-patterned graphene transistor. The same procedure was applied to all other samples. Figure 4a is the cartoon of the photocurrent mapping of the metal nanoparticle decorated graphene device. Figure 4b is the typical photocurrent mapping image of the Ag nanoparticle-patterned graphene transistor with 487 nm laser with 200 nm per step at V_g = 0 V and V_{ds} = 0 V. Figure 4c is the 3D plot of the source and drain electrode along the broken line in Figure 4b. The photocurrent mapping image clearly shows an antisymmetric plot of the source and drain electrode, which is consistent with that reported in the literature.[10,12,26] Contact effects at graphene and metal electrode junctions under zero bias application have been extensively studied.[10,12,14] Photogenerated electron−hole pairs can be separated by the built-in potential at the metal−graphene junction originating from its work function difference, contributing to the measurable photocurrent. Thus, mirror symmetry of the built-in potential profile at each graphene-metal contact produces antisymmetric photocurrent at source and drain electrode, as seen in Figure 4b,c. Modification of built-in potential can benefit improvement of photoresponse in addition to the plasmonic enhancement of photocurrent at the graphene-metal electrode junction because Ag, Au, and Cu nanoparticles induce p-type doping in graphene as discussed in Figure 3b.

According to the literatures,[16,28,30] the working mechanism of our devices which is a hybrid structure of graphene and nanoparticles seems to be based on photoinduced doping (photogating effect) and photovoltaic effect. The photogating effect which is based on light-induced modification of graphene carrier density and thus its conductance $\Delta\sigma = \Delta nq\mu$, where σ is electrical conductivity, q is electron charge, and μ is the mobility. Hot electrons created in the metal nanoparticles by absorbing light can be injected into graphene tunneling through very thin spacer layer of block copolymer. And the intense near field around the decorated metal nanoparticles will enhance the direct excitation of electron−hole (e−h) pairs efficiently in a single graphene layer, and photoexcited e-h pairs will be separated by the built-in electric field formed at the graphene-metal contacts. e−h separation will be the most effective at the graphene−metal contact. Still, measurable photocurrent can be observed at the graphene channel area as seen in Figure 4c, which seems to be originated from photoinduced doping from metal nanoparticles to graphene. Because of the high mobility of graphene, both sources of photon-induced graphene conduction electrons (direct excitation and hot electrons) can flow directly into the electrical circuit and thus can be detected as a photocurrent. Bolometric effect which is based on the change in μ due to heating is different with the photogating effect based on a light-induced change in n.

Recently, Niu et al. reported on the changes in the surface plasmon resonance due to electromagnetic coupling between graphene and Au nanoparticles.[42] In this work, they demonstrated that surface plasmon resonance wavelength was shifted by the variation of the thickness of insulating spacer between graphene and Au nanoparticles. This is attributed to the electromagnetic coupling between the localized surface plasmons excited in the metal nanoparticles and the graphene film. The intensity of the coupling decays exponentially with a decay length of d/R = 0.36, where d is the spacer layer thickness and R is the diameter of the Au nanoparticles. In our system, we used block copolymer spacer (with thickness of >1 nm, as confirmed by XPS) between graphene and Au/Ag nanoparticles. These thin space layers can slightly shift surface plasmon of Au nanoparticles and do not significantly influence on the photogating effect.

By changing the laser wavelength in the visible range between 400 and 700 nm, photocurrent was mapped in the same area at the fixed laser power of 1.08 mW. The photocurrent mapping images of the Ag nanoparticle-patterned graphene transistor at various laser wavelengths were plotted in the same scale, as shown in Figure 4d. The maximum photocurrent enhancement was observed at 446 nm, which is consistent with the optical absorption from localized surface plasmon resonance for Ag nanoparticles shown in Figure 3a. Because the work functions for graphene and Cr are very close,[43] photocurrent generation at the interface between the bare graphene and the electrode was undetectable using the same measurement conditions of the Ag-patterned graphene device shown in Figure 4 (Supporting Information, Figure S5).

After measuring the photocurrent of graphene transistors patterned with single (Ag, Au and Cu), double (Ag−Au), and triple (Ag−Au−Cu) metal particles as a function of the laser wavelength, the responsivity is plotted in Figure 5a,b. The maximum responsivity of the Ag, Au, and Cu metal nanoparticle-patterned graphene is exhibited at ∼450, ∼530,

DOI: 10.1021/ph500412p
ACS Photonics 2015, 2, 506−514

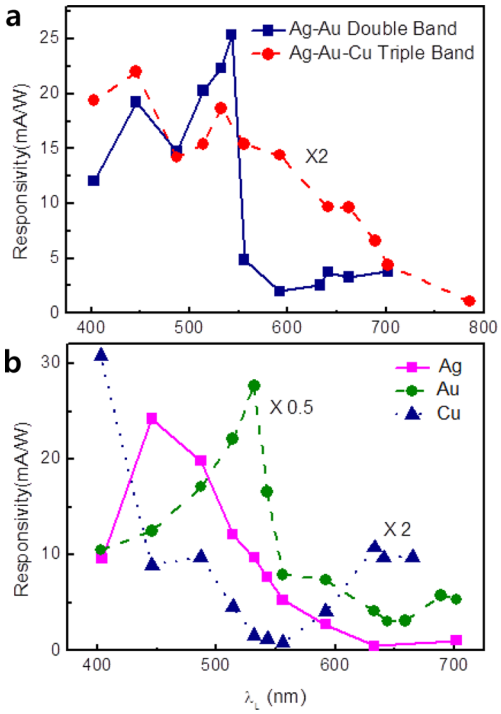

Figure 5. Responsivity of graphene with metal nanoparticle arrays. Responsivity of (a) the double (Ag–Au) and triple band (Ag–Au–Cu) graphene-based photodetectors and (b) the Ag-, Au-, and Cu-patterned graphene-based photodetectors as a function of laser wavelength.

and ~650 nm, respectively, which is consistent with the optical absorption results shown in Figure 3a. However, for Cu nanoparticle-patterned graphene, a large enhancement of the photocurrent is observed at a shorter wavelength. The responsivity at the resonance frequency is ~55, 25, 5 mA/W for Au, Ag and Cu nanoparticle-patterned graphene transistors, respectively. The responsivity of graphene photodetector assisted with Au nanoparticles prepared by a different method was 6.1 mA/W reported in the previous work,[27] which is lower even with higher Au nanoparticle density on graphene than our results by about a factor of 10. For double (Ag–Au) and triple (Ag–Au–Cu) metal nanoparticle-patterned graphene photodetectors, photocurrent enhancement from Ag and Au nanoparticle is clearly observed at ~450 and ~530 nm, respectively. A noticeable enhancement of the photocurrent at longer wavelengths is still observable as shown in Figure 5b, even with sparse wavelengths of the lasers for photocurrent measurement.

It is valuable to mention the effect of the relative concentration of Ag, Au, and Cu metal nanoparticles on the spectral shape of the responsivity to develop plasmon assisted graphene photodetectors. As mentioned earlier in Figure 3a, localized surface plasmon resonance intensity from the nanoparticles exhibited in the order of Ag, Au, and Cu. Ag/Au = 1:3 and Ag/Au/Cu = 2:3:5 were prepared for surface plasmon assisted double- and triple- band graphene photodetectors. Responsivity from Ag nanoparticles from double band (Ag, Au) graphene photodetector at the concentration of Ag/Au = 1:3 was measured to be somewhat lower than that from Au nanoparticles. By increasing Ag concentration in the triple band (Ag, Au, Cu) sample case, photocurrent enhanced from Ag nanoparticles was observed to be increased by about 50% against that from Au nanoparticles compared to double band photodetectors as shown in Figure 3a. Overall, the spectral shape of responsivity from each photodetectors matches well with optical absorbance data. Slight difference between optical absorbance data and spectral shape of responsivity may be related with stability of Ag and Cu nanoparticles which are generally less stable than Au during the measurement scanning with laser.

We extended synthetic route for metallic particles with dual surface plasmonic bands using a different protocol. When we used a solvent mixture of toluene and tetrahydrofuran (THF; toluene/THF = 7/3, v/v) to prepare the PS-*b*-P4VP copolymer solution, spherical and cylindrical micelles were simultaneously formed because the addition of a slightly selective solvent, THF, decreases the solvent selectivity for the copolymers (Supporting Information, Figure S6). Subsequently, the loading of Ag precursors and hydrazine reducing agents to the copolymer micellar solution led to the formation of Ag dots and Ag nanorods as confirmed by HR-TEM images (Supporting Information, Figure S7a,b). The optical absorption of Ag dots and the mixture of Ag dots and nanorods were measured (Supporting Information, Figure S7c). As clearly shown in the figure, a single plasmonic absorption band was detected at approximately 420 nm by the Ag dot arrays, while an additional band was detected at approximately 600 nm, which originated from the formation of Ag nanorods. This method allows the formation of dual plasmonic bands from a single material and single process. Note that Ag particles with different shapes can be easily tuned by controlling the morphologies of the micellar templates.

The case of randomly distributed Ag nanoparticles (6 nm in diameter) and Ag nanorods (6 nm in diameter and 20 nm in length) on graphene was simulated by FDTD simulation. The Ag band was clearly split into two bands (Supporting Information, Figure S8). However, each band was ~50 nm higher than that of the experimental results (shown in Figure S7) as discussed earlier. This approach is very simple and effective, not only providing more than two absorption peaks with a single component, but also providing arrays with fixed separation distances between the dots or rods depending on the molecular weight of the copolymers. Therefore, the plasmonic resonance frequency can be modulated to the desired values. The normalized responsivity of photodetectors of graphene loaded with Ag dots and the mixture of Ag dot and nanorods was measured as a function of the laser wavelength (Supporting Information, Figure S7d). As shown in the figure, a small enhancement of the photocurrent is observed at approximately 600 nm, which originates from the Ag nanorods.

In addition, two different block copolymer micellar solutions containing Au and Ag nanodots reduced by hydrazine reductant can be mixed simultaneously to generate two plasmonic bands (Supporting Information, Figure S9). By modifying the conventional metal nanoparticle patterning process using BCP templates and varying the nanopatterning of metal nanoparticles, the frequency and number of plasmonic resonances can be designed with versatility.

Finally, utilization of uniform patterning of metal nanoparticles by block copolymers can be expanded into other types of graphene photodetectors. Recently, vertically stacked graphene photodetectors consisting of a pair graphene separated by a thin tunnel barrier[29] demonstrated broadband photodetection from the visible to the mid-infrared range by tunneling of photoexcited hot carriers generated in the top

DOI: 10.1021/ph500412p
ACS Photonics 2015, 2, 506–514

layer with responsivity of over 1A/W at mid-infrared. Metal nanoparticle patterning by our method on top graphene layer will provide spectral selectivity and improve responsivity further in this type of vertical graphene photodetectors effectively because whole graphene surface will be involved in photo response by hot-carrier generation under optical illumination.

CONCLUSIONS

Various metal nanoparticle arrays (Ag/Au/Cu) in a regular structure were successfully fabricated on graphene by utilizing block copolymers without any surface treatment. This protocol is very simple and versatile for tuning the plasmonic resonance and for controlling the number of resonances. The photocurrent enhancement assisted by surface plasmonic metal nanoparticles was observed by changing the laser wavelengths from approximately 400 to 800 nm. The resonance phenomenon of photocurrent was well matched with the optical absorption data of metal nanoparticles fabricated on graphene. Graphene-based photodetectors, which are plasmonically enhanced in the red/green/blue region, may be utilized for color filters. Moreover, flexible CMOS image sensors (CIS) can be one of the promising applications of graphene photodetectors assisted with plasmonic enhancement in the near future, which simultaneously fulfills the function of a color filter. By tuning the number and frequency of plasmonic resonances by utilizing block copolymers, multiband or single-band photodetectors of graphene could be utilized in various applications in the future.

METHODS

Synthesis and Transfer Graphene. Graphene was synthesized on a 75 μm thick copper foil by chemical vapor deposition (CVD) at 985 °C by flowing methane (30 sccm) and hydrogen (100 sccm) for 20 min under vacuum (~950 mTorr). The diameter of the CVD chamber (8″) allowed the uniform synthesis of graphene on the ~3 × 3″ copper foil. Hydrogen was injected from the initial point to the cool down (to room temperature) stage, while methane was injected only at the growth temperature. Poly(methyl methacrylate) (PMMA) purchased from Sigma-Aldrich (C4) was spin-coated on graphene grown on a 75 μm thick copper foil at a speed of 1000 rpm for 60 s. Then, the copper was etched away using a nickel etchant for approximately 2 h (Transene Company Inc.). Subsequently, the PMMA-coated graphene layers were rinsed in deionized (DI) water several times. The PMMA-coated graphene was then placed on a Si/SiO_2 (100 nm) substrate and immediately dried in an oven at 80 °C.

Synthesis of Metal Nanoparticle Arrays. The 0.5 wt % polystyrene-*block*-poly(acrylic acid) (PS-*b*-PAA) copolymers (number-average molecular weights M_n^{PS} = 16 kg/mol and M_n^{PAA} = 4.3 kg/mol, polydispersity (M_w/M_n = 1.15) were dissolved in toluene to form spherical micelles consisting of a PS corona and a PAA core. Subsequently, the PS-*b*-PAA thin films were immersed in an aqueous 0.1 wt % $AgNO_3$ solution for 3 min to bind Ag^+ with the PAA chains, which was followed by hydrogen plasma treatment for 12 s in order to reduce Ag^+ to pure Ag nanoparticles. The oleylamine-modified Au nanoparticles were synthesized by a chemical reduction process. Typically, 60 mg of Au precursor ($HAuCl_4 \cdot 3H_2O$) and 1.3 g of oleylamine were dissolved in 1 mL of toluene. This mixture was subsequently injected into a refluxing solution containing 2.5 g of oleylamine dissolved in toluene and held at 110 °C for 2 h. Finally, the Au nanoparticles were collected by repeated precipitation and centrifugation in methanol and were dispersed in toluene. To fabricate quasi-hexagonally ordered Cu nanoparticle arrays, polystyrene-*block*-poly(4-vinylpyridine) (PS-*b*-P4VP) copolymers (number-average molecular weights M_n^{PS} = 35 kg/mol and M_n^{P4VP} = 18.5 kg/mol, dispersity M_w/M_n = 1.15) were dissolved at 80 °C for 3 h, and subsequently, $CuCl_2$ salt (molar ratio of $CuCl_2$/vinylpyridine = 0.8) was added into the polymer solution. After mixing for 6 h, small amounts of aqueous hydrazine were added into the Cu-loaded PS-*b*-P4VP micellar solution to form pure Cu nanoparticles within P4VP cores.

Synthesis of Triple Metal Nanoparticle Arrays on Graphene Transistor. The PS-*b*-PAA spherical micelles were prepared in toluene and mixed with oleylamine-modified Au nanoparticles with a 1:1 weight ratio. Subsequently, PS-*b*-PAA/Au solutions were transferred onto a graphene transistor by spin-coating at 3000 rpm for 60 s, which was followed by immersion in a 0.1% $AgNO_3$(aq) solution for 3 min to bind Ag^+ with the PAA chains. When the films were exposed to hydrogen plasma treatment (Femto Plasma Cleaner, 100 W) for 12 s, hierarchical nanostructured Ag/Au arrays, which can exhibit dual surface plasmon bands, were obtained. To fabricate triple plasmon bands, Cu-containing PS-*b*-P4VP were spin-coated on a graphene transistor with Ag/Au arrays.

Characterization of Metal Nanoparticle Arrays. For transmission electron microscope (TEM) measurements, metal nanoparticle-containing solutions were spin-coated on a Formvar-coated copper grid. The TEM images for general metal nanoparticle patterns were taken in the bright-field mode using JEM-2100 (JEOL, Tokyo, Japan). The scanning TEM (STEM) images were taken in the high-angle annular-dark-field (HAADF) mode of a JEM-2100F (JEOL Ltd.) operating at an acceleration voltage of 200 kV. The ultraviolet−visible-infrared (UV−vis-IR) measurements for localized surface plasmon resonance absorbance were carried out with a Varian Carey 5000 (Agilent) spectrophotometer. All samples used for the UV−vis measurements of surface plasmon resonance were fabricated using glass substrates instead of a graphene transistor.

Device Fabrication and Characterization. The graphene was transferred on Si/SiO_2 (100 nm) by conventional "wet" graphene transfer. A graphene channel was patterned by photolithography followed by oxygen plasma ashing process for 120 s. The photoresist on the graphene channel was removed by soaking in acetone, which was followed by isopropyl alcohol (IPA) rinsing. Finally, the source and drain electrodes (Cr(10 nm)/Au(100 nm)) were patterned using photolithography and a lift-off process. The electrical characterization of graphene devices was conducted with an Agilent 4156C system. The Raman spectra were acquired by a Nanobase (XperRam 200) instrument with a 514 nm laser line. By observing the Raman spectrum of graphene, the synthesis condition of graphene and the metallization condition of the patterned metal precursor by oxygen plasma were finely tuned. The photocurrent mapping was implemented with a modified Raman instrument (XperRam 200) by coupling various lasers using optical fibers with 200 nm per step.

DOI: 10.1021/ph500412p
ACS Photonics 2015, 2, 506−514

■ ASSOCIATED CONTENT

Supporting Information

Detailed materials and methods can be found in the supporting materials of this article. This material is available free of charge via the Internet at http://pubs.acs.org.

■ AUTHOR INFORMATION

Corresponding Authors

*E-mail: spark@unist.ac.kr.

*E-mail: chang-won.lee@samsung.com.

Author Contributions

‡These authors contributed equally (U.J.K. and S.Y.).

Notes

The authors declare no competing financial interest.

■ ACKNOWLEDGMENTS

This research was supported by BK21 Plus funded by the Ministry of Education, Korea (10Z20130011057).

■ REFERENCES

(1) Geim, A. K.; Novoselov, K. S. The rise of graphene. *Nat. Mater.* **2007**, *6*, 183−191.

(2) Chen, J.-H.; Jang, C.; Xiao, S.; Ishigami, M.; Fuhrer, M. S. Intrinsic and extrinsic performance limits of graphene devices on SiO_2. *Nat. Nanotechnol.* **2008**, *3*, 206−209.

(3) Nair, R. R.; Blake, P.; Grigorenko, A. N.; Novoselov, K. S.; Booth, T. J.; Stauber, T.; Peres, N. M. R.; Geim, A. K. Fine structure constant defines visual transparency of graphene. *Science* **2008**, *320*, 1380.

(4) Yang, H.; Heo, J.; Park, S.; Song, H. J.; Seo, D. H.; Byun, K.-E.; Kim, P.; Yoo, I.; Chung, H.-J.; Kim, K. Graphene barristor, a triode device with a gate-controlled Schottky barrier. *Science* **2012**, *336*, 1140−1143.

(5) Zhang, Y.; Tan, Y.-W.; Stormer, H. L.; Kim, P. Experimental observation of the quantum Hall effect and Berry's phase in graphene. *Nature* **2005**, *438*, 201−204.

(6) Li, X.; Zhu, H.; Wang, K.; Cao, A.; Wei, J.; Li, C.; Jia, Y.; Li, Z.; Li, X.; Wu, D. Graphene-on-silicon Schottky junction solar cells. *Adv. Mater.* **2010**, *22*, 2743−2748.

(7) Novoselov, K. S.; Geim, A. K.; Morozov, S. V.; Jiang, D.; Katsnelson, M. I.; Grigorieva, I. V.; Dubonos, S. V.; Firsov, A. A. Two-dimensional gas of massless Dirac fermions in graphene. *Nature* **2005**, *438*, 197−200.

(8) Wang, F.; Zhang, Y.; Tian, C.; Girit, C.; Zettl, A.; Crommie, M.; Shen, Y. R. Gate-variable optical transitions in graphene. *Science* **2008**, *320*, 206−209.

(9) Liu, M.; Yin, X.; Ulin-Avila, E.; Geng, B.; Zentgraf, T.; Ju, L.; Wang, F.; Zhang, X. A graphene-based broadband optical modulator. *Nature* **2011**, *474*, 64−67.

(10) Xia, F.; Mueller, T.; Lin, Y.-M.; Valdes-Garcia, A.; Avouris, P. Ultrafast graphene photodetector. *Nat. Nanotechnol.* **2009**, *4*, 839−843.

(11) Mueller, T.; Xia, F.; Avouris, P. Graphene photodetectors for high-speed optical communications. *Nat. Photonics* **2010**, *4*, 297−301.

(12) Freitag, M.; Low, T.; Xia, F.; Avouris, P. Photoconductivity of biased graphene. *Nat. Photonics* **2013**, *7*, 53−59.

(13) Gabor, N. M.; Song, J. C. W.; Ma, Q.; Nair, N. L.; Taychatanapat, T.; Watanabe, K.; Taniguchi, T.; Levitov, L. S.; Pablo, J.-H. Hot carrier-assisted intrinsic photoresponse in graphene. *Science* **2011**, *334*, 648−652.

(14) Lemme, M. K.; Koppens, F. H. L.; Falk, A. L.; Rudner, M. S.; Park, H.; Levitov, L. S.; Marcus, C. M. Gate-activated photoresponse in a graphene *p*−*n* junction. *Nano Lett.* **2011**, *11*, 4134−4137.

(15) Chen, C.-C.; Aykol, M.; Chang, C.-C.; Levi, A. F. J.; Cronin, S. B. Graphene-silicon Schottky diodes. *Nano Lett.* **2011**, *11*, 1863−1867.

(16) Li, J.; Niu, L.; Zheng, Z.; Yan, F. Photosensitive graphene transistors. *Adv. Mater.* **2014**, *26*, 15239−5273.

(17) Konstantatos, G.; Badioli, M.; Gaudreau, L.; Osmond, J.; Bernechea, M.; de Arquer, F. P. G.; Gatti, F.; Koppens, F. H. L. Hybrid graphene−quantum dot phototransistors with ultrahigh gain. *Nat. Nanotechnol.* **2012**, *7*, 363−368.

(18) Sun, Z.; Liu, Z.; Li, J.; Tai, G. A.; Lau, S. P.; Yan, F. Infrared photodetectors based on CVD-grown graphene and PbS quantum dots with ultrahigh responsivity. *Adv. Mater.* **2012**, *24*, 5878−5883.

(19) Zhang, W.; Chuu, C.-P.; Huang, J.-K.; Chen, C.-H.; Tsai, M.-L.; Chang, Y.-H.; Liang, C.-T.; Chen, Y.-Z.; Chueh, Y.-L.; He, J.-H.; Chou, M.-Y.; Li, L.-J. Ultrahigh-gain photodetectors based on atomically thin graphene-MoS_2 heterostructures. *Sci. Rep.* **2014**, *4*, 3826.

(20) Gan, X.; Shiue, R.-J.; Gao, Y.; Meric, I.; Heinz, T. F.; Shepard, K.; Hone, J.; Assefa, S.; Englund, D. Chip-integrated ultrafast graphene photodetector with high responsivity. *Nat. Photonics* **2013**, *7*, 883−887.

(21) Wang, X.; Cheng, Z.; Xu, K.; Tsang, H. K.; Xu, J.-B. High-responsivity graphene/silicon-heterostructure waveguide photodetectors. *Nat. Photonics* **2013**, *7*, 888−891.

(22) Pospischil, A.; Humer, M.; Furchi, M. M.; Bachmann, D.; Guider, R.; Fromherz, T.; Mueller, T. CMOS-compatible graphene photodetector covering all optical communication bands. *Nat. Photonics* **2013**, *7*, 892−896.

(23) Liu, C.-H.; Chang, Y.-C.; Norris, T. B.; Zhong, Z. Graphene photodetectors with ultra-broadband and high responsivity at room temperature. *Nat. Nanotechnol.* **2014**, *9*, 273−278.

(24) Chang, H.; Sun, Z.; Saito, M.; Yuan, Q.; Zhang, H.; Li, J.; Wang, Z.; Fujita, T.; Ding, F.; Zheng, Z. Regulating infrared photoresponses in reduced graphene oxide phototransistors by defect and atomic structure control. *ACS Nano* **2013**, *7*, 6310−6320.

(25) Xu, X.; Gabor, N. M.; Alden, J. S.; Zande, A. M.; McEuen, P. L. Photo-thermoelectric effect at a graphene interface junction. *Nano Lett.* **2010**, *10*, 562−566.

(26) Echtermeyer, T. J.; Britnell, L.; Jasnos, P. K.; Lombardo, A.; Gorbachev, R. V.; Grigorenko, A. N.; Geim, A. K.; Ferrari, A. C.; Novoselov, K. S. Strong plasmonic enhancement of photovoltage in graphene. *Nat. Commun.* **2011**, *2*, 458.

(27) Liu, Y.; Cheng, R.; Liao, L.; Zhou, H.; Bai, J.; Liu, G.; Liu, L.; Huang, Y.; Duan, X. Plasmon resonance enhanced multicolour photodetection by graphene. *Nat. Commun.* **2011**, *2*, 579.

(28) Fang, Z.; Liu, Z.; Wang, Y.; Ajayan, P. M.; Nordlander, P.; Halas, N. J. Graphene-antenna sandwich photodetector. *Nano Lett.* **2012**, *12*, 3808−3813.

(29) Zhang, T.; Liu, T.; Meng, B.; Li, X.; Liang, G.; Hu, X.; Wang, Q. J. Broadband high photoresponse from pure monolayer graphene photodetector. *Nat. Commun.* **2013**, *4*, 1811.

(30) Koppens, F. H. L.; Mueller, T.; Avouris, P.; Ferrari, A. C.; Vitiello, M. S.; Polini, M. Photodetectors based on graphene, other two-dimensional materials and hybrid systems. *Nat. Nanotechnol.* **2014**, *9*, 780−793.

(31) Riess, G. Micellization of block copolymers. Micellization of block copolymers. *Prog. Polym. Sci.* **2003**, *28*, 1107−1170.

(32) Kim, S. O.; Solak, H. H.; Stoykovich, M. P.; Ferrier, N. J.; Pablo, J. J.; Nealey, P. F. Epitaxial self-assembly of block copolymers on lithographically defined nanopatterned substrates. *Nature* **2003**, *424*, 411−414.

(33) Park, S.; Lee, D. H.; Xu, J.; Kim, B.; Hong, S. W.; Jeong, U.; Xu, T.; Russell, T. P. Macroscopic 10-terabit-per-square-inch arrays from block copolymers with lateral order. *Science* **2009**, *323*, 1030−1033.

(34) Bennett, R. D.; Xiong, G. Y.; Ren, Z. F.; Cohen, R. E. Using block copolymer micellar thin films as templates for the production of catalysts for carbon nanotube growth. *Chem. Mater.* **2004**, *16*, 5589−5595.

(35) Fanizza, E.; Depalo, N.; Clary, L.; Agostiano, A.; Striccoli, M.; Curri, M. L. A combined size sorting strategy for monodisperse plasmonic nanostructures. *Nanoscale* **2013**, *5*, 3272−3282.

(36) Park, S.; Wang, J.-Y.; Kim, B.; Russell, T. P. From nanorings to nanodots by patterning with block copolymers. *Nano Lett.* **2008**, *8*, 1667−1672.

DOI: 10.1021/ph500412p
ACS Photonics 2015, 2, 506−514

(37) Mistark, P. A.; Park, S.; Yalcin, S. E.; Lee, D. H.; Yavuzcetin, O.; Tuominen, M. T.; Russell, T. P.; Achermann, M. Block-copolymer-based plasmonic nanostructures. *ACS Nano* **2009**, *3*, 3987−3992.
(38) Petrucci, R. H.; Harwood, W. S.; Herring, G. E.; Madura, J. *General Chemistry: Principles and Modern Applications*, 9th ed.; Pearson Education: Upper Saddle River, NJ, 2007.
(39) Hutter, E.; Fendler, J. H. Exploitation of localized surface plasmon resonance. *Adv. Mater.* **2006**, *16*, 1685−1706.
(40) Taflove, A.; Hagness, S. C. *Computational Electrodynamics: The Finite-Difference Time-Domain Method*, 3rd ed.; Artech House Publishers: London, 2005.
(41) Giovannetti, G.; Khomyakov, P. A.; Brocks, G.; Karpan, V. M.; Brink, J.; Kelly, P. J. Doping graphene with metal contacts. *Phys. Rev. Lett.* **2008**, *101*, 026803.
(42) Niu, J.; Shin, Y. J.; Son, J.; Lee, Y.; Ahn, J.-H.; Yang, H. Shifting of surface plasmon resonance due to electromagnetic coupling between graphene and Au nanoparticles. *Opt. Express* **2012**, *20*, 19690−19696.
(43) Michaelson, H. B. The work function of elements and its periodicity. The work function of elements and its periodicity. *J. Appl. Phys.* **1977**, *48*, 4729−4733.

DOI: 10.1021/ph500412p
ACS Photonics 2015, 2, 506−514